

# Chemical Science

Accepted Manuscript



This article can be cited before page numbers have been issued, to do this please use: H. Zhong, Y. Wang, C. Cui, F. Zhou, S. Hu and R. Wang, *Chem. Sci.*, 2018, DOI: 10.1039/C8SC03531H.



This is an Accepted Manuscript, which has been through the Royal Society of Chemistry peer review process and has been accepted for publication.

Accepted Manuscripts are published online shortly after acceptance, before technical editing, formatting and proof reading. Using this free service, authors can make their results available to the community, in citable form, before we publish the edited article. We will replace this Accepted Manuscript with the edited and formatted Advance Article as soon as it is available.

You can find more information about Accepted Manuscripts in the [author guidelines](#).

Please note that technical editing may introduce minor changes to the text and/or graphics, which may alter content. The journal's standard [Terms & Conditions](#) and the ethical guidelines, outlined in our [author and reviewer resource centre](#), still apply. In no event shall the Royal Society of Chemistry be held responsible for any errors or omissions in this Accepted Manuscript or any consequences arising from the use of any information it contains.

# Facile fabrication of Cu-based alloy nanoparticles encapsulated within hollow octahedral N-doped porous carbon for selective oxidation of hydrocarbons

Hong Zhong,<sup>ab</sup> Yangxin Wang,<sup>a</sup> Caiyan Cui,<sup>a</sup> Feng Zhou,<sup>a</sup> Shuangqi Hu<sup>b</sup> and Ruihu Wang<sup>\*a</sup>

Received 00th January 20xx,  
Accepted 00th January 20xx

DOI: 10.1039/x0xx00000x

www.rsc.org/

Hollow carbon materials with versatile chemical compositions and complicated shell architectures hold great promises in heterogeneous catalysis, it is a daunting challenge to synthesize metal alloy nanoparticles (NPs) supported by the hollow nanostructures. Herein, we present a simple approach for facile fabrication of Pd-Cu alloy NPs embedded in hollow octahedral N-doped porous carbon (Pd-Cu@HO-NPC). The hollow material is derived from HKUST-1 coated by imidazolium-based ionic polymer (ImIP). Water-sensitive HKUST-1 is simultaneously removed in the process of anion exchange between bromide in the ImIP shell and tetrachloropalladate in aqueous medium. The released Cu(II) ions and exchanged Pd(II) ions serve as Cu and Pd sources in subsequent pyrolysis. The resultant Pd-Cu@HO-NPC exhibits high catalytic activity, selectivity, stability and recyclability in the aerobic oxidation of hydrocarbons. More attractively, the synthetic strategy is of excellent generality, and could be extended to the synthesis of Cu-based bimetallic and trimetallic alloy NPs, such as Pt-Cu@HO-NPC and Pd-Pt-Cu@HO-NPC. This work highlights the superiority of water-sensitive metal-organic frameworks in the ingenious design of hollow carbon materials incorporated with well-dispersed metal alloy NPs.

## Introduction

Supported metal nanocatalysts have captured increasing interests in fine chemical industry, environmental protection and energy conversion.<sup>1-4</sup> Hollow carbon materials with large internal voids and porous shells are one type of promising supports of metal nanoparticles (NPs).<sup>5-8</sup> The shell could function as a barrier to prevent coalescence of the embedded metal NPs, and the pores in the shell could provide a highway for free diffusion of substrates to access metal active sites.<sup>5,9-11</sup> Considerable progresses have been achieved in the preparation of hollow porous materials,<sup>12-14</sup> and the application of several hollow nitrogen-doping carbon materials incorporated with noble metal NPs has also been explored in heterogeneous catalysis.<sup>6,15</sup> Alloying a parent noble metal with a non-precious metal holds a great promise to improve the catalytic performance and minimize the usage of noble metals,<sup>16,17</sup> but metal alloy NPs supported by hollow carbon materials have not been reported owing to their the complicated fabrication processes with harsh reaction conditions and/or the use of expensive additives. It is highly

desirable to develop a simple yet effective strategy to integrate metal alloy NPs into hollow heteroatom-doped carbon materials for the design of advanced nanocatalysts.

The templating methods are considered as straightforward and versatile approaches for the synthesis of hollow carbon nanostructures,<sup>18-20</sup> the compatibility between template surface and carbon precursors has pivotal influences on the homogeneity of carbon shells and the dispersion of metal NPs.<sup>5</sup> The deliberate selection and modification of carbon precursors play crucial roles in the final physical and chemical properties of resulting carbon shells.<sup>21</sup> In the context, the main-chain imidazolium-based ionic polymers (ImIPs) are one type of promising precursors to synthesize heteroatom-doped carbon materials. The counter halide anions could facilitate exchange with various heteroatom-containing and/or metal-containing anions,<sup>22-24</sup> which provides great opportunities to control the loading amount and the types of metal precursors in ImIPs. Metal and/or metal alloy NPs could be expected after subsequent pyrolysis without the extra addition of other heteroatoms and metal ions. Importantly, ImIPs could serve as robust physical barriers to effectively resist the sintering of metal NPs during pyrolysis, resulting in uniform distribution and high dispersion of metal NPs. The incorporated heteroatoms in the carbon lattice not only modify their chemical and electrical properties, but also enhance the interactions between the carbon support and the embedded metal NPs to trigger superior catalytic performance.<sup>14</sup> Despite these attractive advantages, as far as we are aware, there is no report on ImIPs-based hollow materials, one of main reasons is

<sup>a</sup> State Key Laboratory of Structural Chemistry, Fujian Institute of Research on the Structure of Matter, Chinese Academy of Sciences, Fuzhou, Fujian 350002, China. E-mail: ruihu@fjirsm.ac.cn

<sup>b</sup> School of Environmental and Safety Engineering, North University of China, Taiyuan 030051, China.

† Electronic Supplementary Information (ESI) available: [details of any supplementary information available should be included here]. See DOI: 10.1039/x0xx00000x



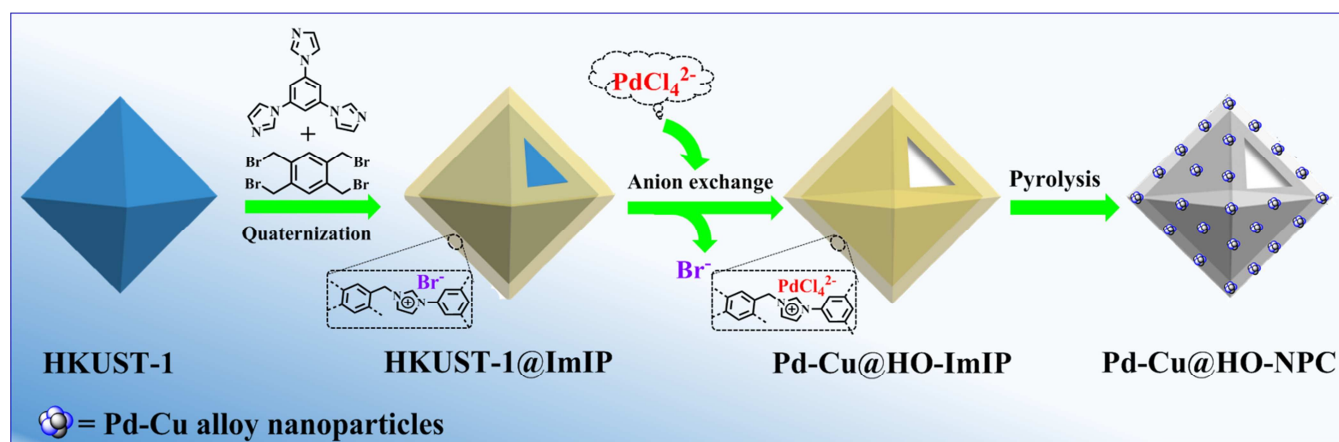
that the flexible backbone of ImIPs is liable to deformation and even collapse after the removal of templates. It is a daunting challenge to construct hollow ImIPs for promising application as the precursors of supported metal nanocatalysts.

Metal-organic frameworks (MOFs), assembled by metal ions/clusters and organic ligands, are suitable templates for the construction of hollow structures owing to their facile synthesis, fascinating morphologies, various compositions and tuneable particle sizes.<sup>25,26</sup> Although MOFs have been extensively used as sacrificial templates to fabricate hollow metal and/or metal oxide composites,<sup>27-30</sup> hollow carbon materials derived from MOFs templates have been rarely reported, more efforts are needed to explore the advantages of MOFs templates in the synthesis of hollow carbon materials with versatile chemical compositions and complicated shell architectures. It is well known that most of MOFs are instable in water, the instability provides tremendous opportunity for disassembly of MOFs cores in MOF@ImIP core-shell structures during anionic exchange of ImIPs under mild conditions, requiring no additional procedures for the removal of MOFs templates.<sup>31,32</sup> The released metal ions and organic ligands could be located in the pores of the hollow shell, which not

only sustains the original shape of ImIPs shells, but also serves as the precursors of carbon and/or metal NPs. After the carbonization, the hollow ImIPs containing modifiable metal ions and heteroatoms could be topotactically transformed into heteroatom-doped porous carbon materials containing homogeneously embedded metal alloy NPs, which brings out unique chemical and physical properties that are not attainable from single MOF or ImIPs precursors.

As a proof-of-concept study, herein, we developed a facile and versatile method for the synthesis of well-dispersed M-Cu alloy NPs embedded in hollow octahedral nitrogen-doped porous carbon (M-Cu@HO-NPC, M = Pd, Pt and Pd-Pt) using water-sensitive HKUST-1 as a template. They were readily prepared through topotactic transformation of hollow M-Cu@HO-ImIPs, which were obtained through anion exchange of core-shell-structured HKUST-1@ImIP with metal-containing anions in water. To the best of our knowledge, this is first report about metal alloy NPs supported by hollow nitrogen-doped carbon materials. Pd-Cu@HO-NPC exhibits high catalytic activity, selectivity and recyclability in the oxidation of hydrocarbons using air as an oxidant in the absence of co-catalysts and additives.

## Results and Discussion



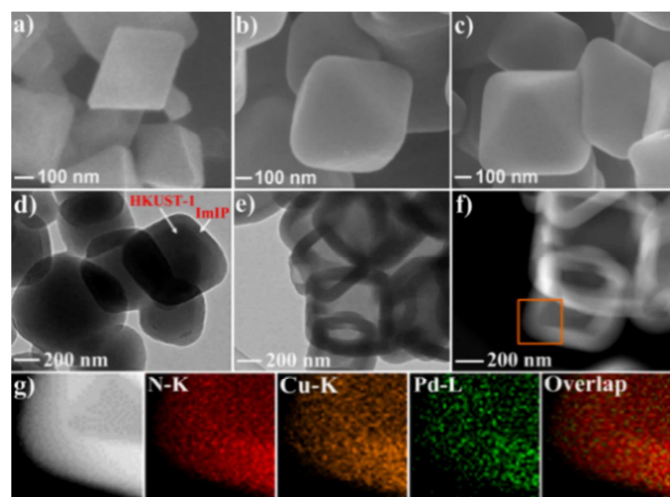
Scheme 1. Schematic illustration for the synthesis of Pd-Cu@HO-NPC.

HKUST-1 has been widely employed as a self-sacrificial template in the preparation of metal oxide composites,<sup>33,34</sup> but its application in the synthesis of hollow carbon materials has not reported so far. As shown in Scheme 1, HKUST-1 was prepared through the assembly of 1,3,5-benzenetricarboxylic acid ( $H_3BTC$ ) and  $Cu(NO_3)_2 \cdot 3H_2O$ .<sup>35</sup> ImIP was readily coated on the surface of HKUST-1 through the quaternization reaction of 1,2,4,5-tetrakis(bromomethyl)benzene and 1,3,5-tri(1H-imidazol-1-yl)benzene to give rise to HKUST-1@ImIP core-shell material, subsequent anion exchange between bromide in the ImIP shell and tetrachloropalladate generated hollow Pd-Cu@HO-ImIP, in which the HKUST-1 template was decomposed simultaneously during anion exchange, no tedious steps and hazardous reagents were employed for the removal of templates when compared with conventional hard-template methods.<sup>5,6,12</sup>

Scanning electron microscopy (SEM) images reveal that HKUST-1 is octahedron-shaped nanocrystals with the edge lengths in the range from 200 to 400 nm (Fig. 1a). After coated with ImIP, the octahedral morphology is retained in HKUST-1@ImIP, but the edge lengths are increased to 300-600 nm (Fig. 1b). Thus, the thickness of the ImIP shell in HKUST-1@ImIP is in the range of 50-100 nm. Notably, the morphology and size of Pd-Cu@HO-ImIP are almost identical with that of HKUST-1@ImIP, indicating the shell structure is well maintained after the decomposition of HKUST-1 (Fig. 1c). Transmission electron microscopy (TEM) images show that HKUST-1@ImIP possesses an octahedral core-shell structure (Fig. 1d). ImIP is homogeneously coated on the surface of HKUST-1 nanocrystals with a thickness of 50-100 nm, which is consistent with the SEM results. Interestingly, Pd-Cu@HO-ImIP exhibits a hollow octahedral structure (Fig. 1e), no HKUST-1



residues are observed. The shape and size of the inner cavity are matched well with those of the original HKUST-1 nanocrystals, no structural collapse and/or deformation are observed in the external shells after the removal of kernel template. To the best of our knowledge, this is first report about hollow ionic polymers with flexible backbones. The outstanding stability of hollow Pd-Cu@HO-ImIP is probably attributed to the assistance of released metal ions and organic ligands from HKUST-1, they reside in the pores of the shell through electrostatic and coordination interactions to sustain the original shape of hollow ImIP shells.<sup>22,36</sup> Notably, the hollow octahedral structure was dramatically squashed when Pd-Cu@HO-ImIP was washed with aqueous EDTA-2Na solution to remove metal ions (Fig. S1†). The high-annular dark-field scanning TEM (HAADF-STEM) images further confirm hollow octahedral structure of Pd-Cu@HO-ImIP (Fig. 1f). The corresponding element mapping images show that Cu (orange) and Pd (green) are co-existent in the octahedral shell (Fig. 1g), they are derived from exchanged tetrachloropalladate ions and released Cu<sup>2+</sup> ions in HKUST-1, respectively. The distribution between Pd and Cu is identical with each other, which is conducive to *in situ* growth of Pd-Cu alloy NPs during subsequent pyrolysis.<sup>22</sup>

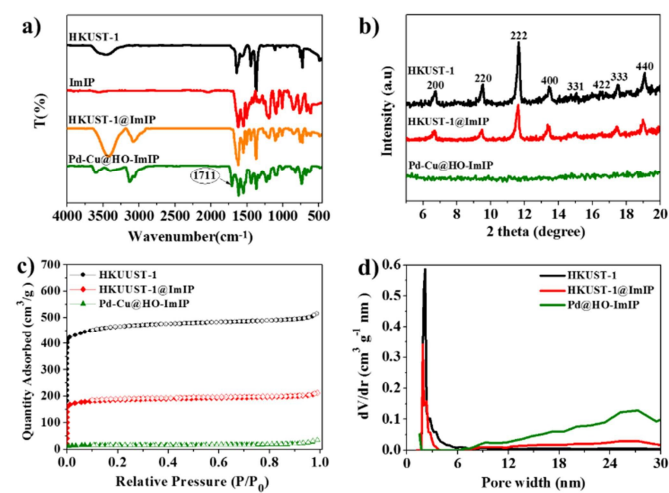


**Fig. 1** SEM images for (a) HKUST-1, (b) HKUST-1@ImIP and (c) Pd-Cu@HO-ImIP. (d) TEM image of HKUST-1@ImIP. (e) TEM image, (f) HAADF-STEM and (g) EDX mapping images of Pd-Cu@HO-ImIP.

In the Fourier-transform infrared (FTIR) spectrum of HKUST-1@ImIP, the simultaneous appearance of the characteristic peaks of HKUST-1 and ImIP reveals their successful combination in the core-shell material (Fig. 2a). An extra peak at 1711 cm<sup>-1</sup>, which corresponds to the carboxylate group of BTC,<sup>35</sup> occurs in the FTIR spectrum of Pd-Cu@HO-ImIP, indicating the decomposition of HKUST-1 and the incorporation of the released BTC into the polymer shell, which serves as adsorption site of Cu(II). Thermogravimetric analysis (TGA) curves show that HKUST-1@ImIP possesses a lower thermal stability than HKUST-1 owing to the presence of the ImIP shell, and Pd-Cu@HO-ImIP begins to decompose after 200 °C (Fig. S2†).<sup>22</sup> Powder X-ray diffraction (XRD) patterns indicate that the crystallinity of HKUST-1 is well retained in

HKUST-1@ImIP (Fig. 2b),<sup>35</sup> no additional diffraction peaks from the ImIP shell are detected. However, the characteristic diffraction peaks of HKUST-1 totally disappear in the XRD pattern of Pd-Cu@HO-ImIP, which further reveals that the decomposition of HKUST-1 octahedral nanocrystals after anion exchange.

The porous properties of HKUST-1, HKUST-1@ImIP and Pd-Cu@HO-ImIP were investigated by N<sub>2</sub> adsorption/desorption at 77 K (Fig. 2c). A rapid nitrogen uptake at very low relative pressure ( $P/P_0 < 0.01$ ) in HKUST-1 and HKUST-1@ImIP indicates that the presence of extensive micropores,<sup>37</sup> while the nitrogen uptake in Pd-Cu@HO-ImIP is negligible. The BET surface areas of HKUST-1 and HKUST-1@ImIP are 1776 and 816 m<sup>2</sup>/g, respectively. As expected, the BET surface area of Pd-Cu@HO-ImIP is as low as 37 m<sup>2</sup> g<sup>-1</sup> owing to both the flexibility of ImIP shell and the pores filling by metal ions and counter anions.<sup>22</sup> The pore size distribution reveals that the predominant pores in HKUST-1 and HKUST-1@ImIP are micropores (Fig. 2d), while the pores in Pd-Cu@HO-ImIP are in the range of mesopores, which are consistent with the results of their nitrogen adsorption-desorption isotherms.



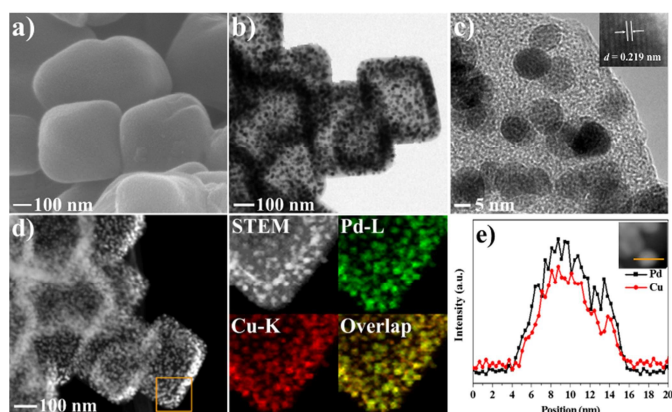
**Fig. 2** (a) FTIR spectra, (b) XRD patterns, (c) N<sub>2</sub> adsorption/desorption isotherms and (d) pore size distribution for HKUST-1, HKUST-1@ImIP and Pd-Cu@HO-ImIP.

Considering unique hollow octahedral structure, high concentrations of carbon and nitrogen species as well as homogeneous distribution of Pd and Cu in Pd-Cu@HO-ImIP, its topotactic transformation at 500 °C under an inert atmosphere gave rise to hollow octahedral nitrogen-doped porous carbon incorporated with Pd-Cu alloy NPs (Pd-Cu@HO-NPC). SEM and TEM analyses indicate that Pd-Cu@HO-NPC possesses a similar hollow octahedral morphology to Pd-Cu@HO-ImIP (Fig. 3), but the edge lengths and the shell thickness are decreased to 250–500 nm and 30–60 nm, respectively, which is probably attributed to volume shrinking during pyrolysis.<sup>38,39</sup> HAADF-STEM images of Pd-Cu@HO-NPC further confirm the maintenance of the hollow structure with an octahedral cavity (Fig. 3d). The metal NPs in the carbon shells are assigned to Pd-Cu alloy formed by the co-reduction of Pd and Cu cations during pyrolysis. The average size of well-dispersed Pd-Cu alloy NPs is 8.2 ± 0.8 nm (Fig. S3†), which is comparable with those





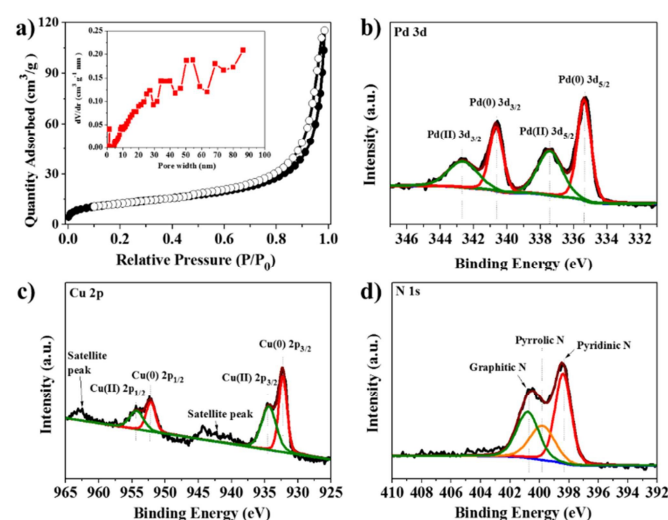
in metal NPs prepared through the pyrolysis of carbon precursors without using extra reductive agents.<sup>6,40</sup> Notably, Pd-Cu alloy NPs are uniformly embedded in the porous carbon shell, no metals NPs are observed on the exterior surface of the carbon shell and/or in the hollow cavity, which is conducive to suppressing the leaching and agglomeration of active species in the catalytic reactions.<sup>6</sup> The corresponding element mapping images show that the distribution between Pd and Cu is identical with each other, revealing the alloying state of bimetallic Pd-Cu NPs, which is further demonstrated by their line-scan analyses (Fig. 3e). The high-resolution TEM image shows the intervals between adjacent lattice fringes are 0.219 nm (Fig. 3c), which corresponds to the (111) lattice plane of Pd-Cu alloy.<sup>41</sup> In the XRD pattern of Pd-Cu@HO-NPC (Fig. S4†), the diffraction peaks at 41.1, 48.2, 69.7 and 83.9 can be indexed as the (111), (200), (220) and (311) facets of face-centered cubic (fcc) Pd-Cu alloy, respectively.<sup>42,43</sup> Inductively coupled plasma (ICP) analyses show that Cu and Pd contents are 0.83 and 0.39 mmol·g<sup>-1</sup>, respectively. The N content in Pd-Cu@HO-NC is 5.8 mmol·g<sup>-1</sup> as determined by elemental analysis.



**Fig. 3** (a) SEM image, (b, c) TEM images, (d) HAADF-STEM and EDX mapping images, and (e) the line-scan analyses of Pd-Cu@HO-NPC.

The N<sub>2</sub> adsorption/desorption isotherms and relevant pore size distribution show that Pd-Cu@HO-NPC possesses predominantly mesopores (Fig. 4a), the BET surface area and total pore volume are 121 m<sup>2</sup> g<sup>-1</sup> and 0.21 cm<sup>3</sup> g<sup>-1</sup>, respectively. The combination of the mesopores with large hollow cavity generated by the self-sacrificial HKUST-1 is favorable for mass transfer, resulting in ready availability of the catalytic active sites to substrate molecules and rapid release of the products in heterogeneous catalytic reaction.<sup>20</sup> The surface composition and valence state of Pd-Cu@HO-NPC were examined by X-ray photoelectron spectroscopy (XPS) measurements. In the XPS survey spectrum (Fig. S5†), the binding energy peaks around 284.1, 335.9, 399.7, 532.0 and 931.9 eV are assigned to C 1s, Pd 3d, N 1s, O 1s and Cu 2p, respectively.<sup>44</sup> The deconvolution of Pd 3d XPS spectrum presents two sets of double peaks corresponding to Pd 3d<sub>5/2</sub> and Pd 3d<sub>3/2</sub> (Fig. 4b). The binding energy peaks at 335.34 and 340.68 eV correspond to Pd(0) 3d<sub>5/2</sub> and 3d<sub>3/2</sub>, respectively, while the peaks at 337.44 and 342.68 eV are attributed to Pd(II) species. The ratio of surface

Pd(0) to Pd(II) is 1.26 as determined by the ratio of their relative peak areas. In Cu 2p XPS spectrum, two sets of double peaks are ascribed to Cu 2p<sub>3/2</sub> and Cu 2p<sub>1/2</sub> of Cu(0) and Cu(II) species, respectively (Fig. 4c). The binding energy peaks at 932.18 and 957.23 eV are assigned to Cu(0) 2p<sub>3/2</sub> and 2p<sub>1/2</sub>, respectively, while the peaks at 934.61 and 954.40 eV correspond to Cu(II) 2p<sub>3/2</sub> and 2p<sub>1/2</sub>, respectively. Impressively, the Pd(0) 3d<sub>5/2</sub> and Cu(0) 2p<sub>3/2</sub> peaks shift negatively by 0.06 and 0.11 eV, respectively, when compared with those in free Pd (335.4 eV) and Cu (932.29 eV).<sup>45</sup> The negative shift probably results from the strong interaction between Pd-Cu alloy NPs and nitrogen-doped carbon, which makes Pd(0) and Cu(0) species more electron-rich than free Pd and Cu.<sup>14</sup> In the high-resolution N 1s XPS spectrum (Fig. 4d), the presence of pyridinic N (398.5 eV), pyrrolic N (399.7 eV) and graphitic N (401.1 eV) could be clearly identified.<sup>46</sup> Raman spectrum shows the characteristic D-band and G-band at 1345 and 1577 cm<sup>-1</sup>, respectively (Fig. S6†). The relative ratio of I<sub>D</sub>/I<sub>G</sub> is 0.98, indicating that the carbon species in Pd-Cu@HO-NPC possess a high graphitization degree, which is favorable for electron mobility and stabilization of the reactive intermediates in the radical-involved catalytic systems.<sup>47</sup>



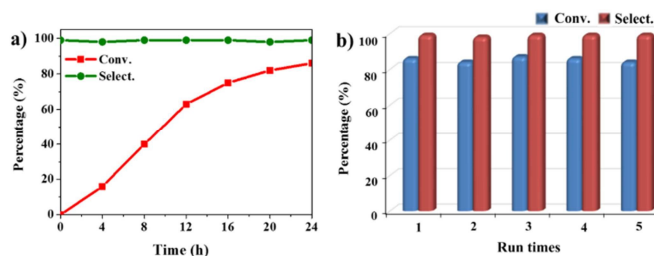
**Fig. 4** (a) N<sub>2</sub> adsorption/desorption isotherms and pore size distribution (inset), (b) Pd 3d, (c) Cu 2p and (d) N 1s XPS spectra for Pd-Cu@HO-NPC.

The attractive advantages of the hollow octahedral nanostructure incorporated with well-dispersed Pd-Cu alloy NPs have encouraged us to explore its catalytic application. The selective oxidation of hydrocarbons is an essential reaction in organic synthesis and industrial chemistry, it has usually required the use of various oxidants, such as toxic metal oxides, peroxides and ozone.<sup>48</sup> Compared with those oxidants, air is undoubtedly the most ubiquitous, atom-economical and environmentally benign oxidant. However, air is unreactive and difficult to activate strong sp<sup>3</sup> C-H bonds of hydrocarbon in the transformation. Recently, various supported noble metal nanocatalysts, such as palladium, platinum, ruthenium and gold, have been reported in selective oxidation of hydrocarbons, but the catalytic systems are subjected to high temperatures, high pressures and/or the use



of the additives.<sup>47,49-51</sup> Alloying a parent noble metal with a second metal offers numerous opportunities to improve catalytic activities, but the application of alloy metal NPs in this chemical transformation has seldom been reported.<sup>52</sup>

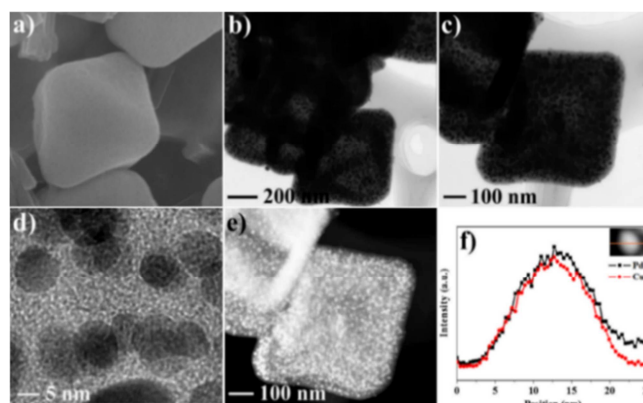
The oxidation of indane was evaluated initially using air as an oxidant in the presence of 0.2 mol% palladium under solvent-free conditions. Kinetic profiles show that indane consumption and 1-indanone formation increased rapidly in the first 8 h, and 86 % conversion of indane was achieved in 24 h (Fig. 5a). The selectivity of 1-indanone remains above 99% in the entire catalytic process. The control experiments were also performed. When the indane oxidation was carried out either in the absence of Pd-Cu@HO-NPC (Table 1, entry 2) or under N<sub>2</sub> atmosphere (entry 3), negligible product was detected in 24 h. As expected, the indane conversion decreased to 50% when hollow Pd-Cu@HO-NPC was replaced by dense Pd-Cu@NPC (entry 4). The use of the commercial Pd/C afforded a 33 % conversion of indane under the same conditions (entry 5). The heterogeneous behavior of this catalytic system was verified by hot filtration experiment. After the reaction was carried out for 6 h, the catalyst was quickly removed by filtration, and the reaction of the filtrate was continued for additional 18 h, both conversion and selectivity show negligible variation (entries 6 and 7).



**Fig. 5** (a) The kinetic curve and (b) recyclability for Pd-Cu@HO-NPC in the oxidation reaction of indane. Reaction conditions: indane (8.77 mmol), catalyst ([Pd] = 0.2 mol%), air flow (5 mL min<sup>-1</sup>), 120 °C and 24 h.

Pd-Cu@HO-NPC shows excellent recyclability and stability in the aerobic oxidation of indane. After the reaction finished, the catalyst was separated by centrifugation, and directly used for next run. Pd-Cu@HO-NPC could be used at least five runs without detectable loss of catalytic activity and selectivity (Fig. 5b), the total turnover number (TON) exceeds 2125. The recovered Pd-Cu@HO-NPC after the consecutive reaction for five runs is denoted as Pd-Cu@HO-NPC-5run. As shown in Fig. 6 and S7†, the Raman spectrum, SEM and TEM images of Pd-Cu@HO-NPC-5run are almost identical with that of as-prepared sample. The most strikingly, Pd-Cu alloy NPs are still uniformly embedded in hollow carbon material with the retention of their original size (Fig. S8†), there are no metals NPs on the exterior of the porous carbon shell and/or in the hollow cavity. Inductively coupled plasma (ICP) analyses show Pd and Cu contents in Pd-Cu@HO-NPC-5run are the same as those in as-synthesized catalyst. These results have demonstrated that hollow HO-NPC could effectively inhibit the leaching of catalytic active species and prevent the

aggregation and migration of Pd-Cu alloy NPs in the hydrocarbon oxidation.



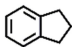
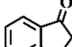
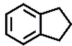
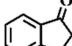
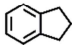
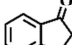
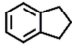
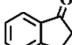
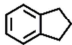
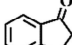
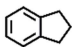
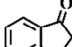
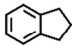
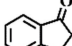
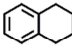
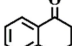
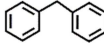
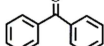
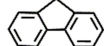
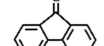
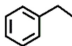
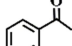
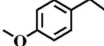
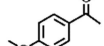
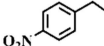
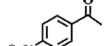

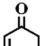
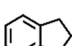
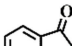
**Fig. 6** (a) SEM, (b, c, d) TEM, (e) HAADF-STEM images and (f) the line-scan analyses for Pd-Cu@HO-NPC-5run.

To extend application scope of the catalytic system, the oxidation reactions of various hydrocarbons were examined using air as an oxidant. As shown in Table 1, a conversion of 75 % was obtained in the oxidation of tetralin, a key intermediate in the commercial production of  $\alpha$ -naphthol (entry 8).<sup>48,52</sup> Diphenylmethane and fluorene with a large molecular size could be transformed into diphenylmethanone and fluorenone in good conversions of 71 % and 89 %, respectively (entries 9 and 10). Impressively, the C-H bond of ethylbenzene was also selectively oxidized, acetophenone was obtained in a 38 % GC yield (entry 11). The electron-rich 1-ethyl-4-methoxybenzene and electron-deficient 1-ethyl-4-nitrobenzene provided the corresponding products in 44 % and 29 % GC yields, respectively (entries 12 and 13), indicating the electron-donating groups in ethylbenzene are more favorable for C-H bond activation than the electron-withdrawing groups in this catalytic system. Besides aromatic molecules, Pd-Cu@HO-NPC is also effective for the oxidation of aliphatic molecules. 48 % conversion and 89 % selectivity were achieved in 24 h when cyclohexene was used as a substrate (entry 14). These results show that Pd-Cu@HO-NPC is a promising catalyst for the aerobic oxidation of allylic- or benzyl sp<sup>3</sup> C-H bonds. Interestingly, when the oxidation of indane was tested in the presence of *p*-benzoquinone, which is a typical radical scavenger. The reaction was totally suppressed to give a negligible conversion (entry 15), indicating that the reaction proceeds through radical intermediates. The attractive catalytic performance of Pd-Cu@HO-NPC in selective aerobic oxidation of hydrocarbons is mainly attributed to its favorable structure features: 1) The hollow cavity and mesoporous shell are beneficial for mass transfer/diffusion of substrates and products; 2) The uniform distribution of Pd-Cu alloy NPs in mesoporous shell makes them readily interact with hydrocarbons and oxygen molecules; 3) The incorporation of nitrogen atoms into carbon shell not only makes Pd-Cu alloy NPs electron-rich, but also significantly enhances the interactions between the carbon shell and the embedded metal NPs; 4) The high graphitization of the carbon shell



benefits the electron mobility and radical stabilization during catalytic oxidation of hydrocarbons.

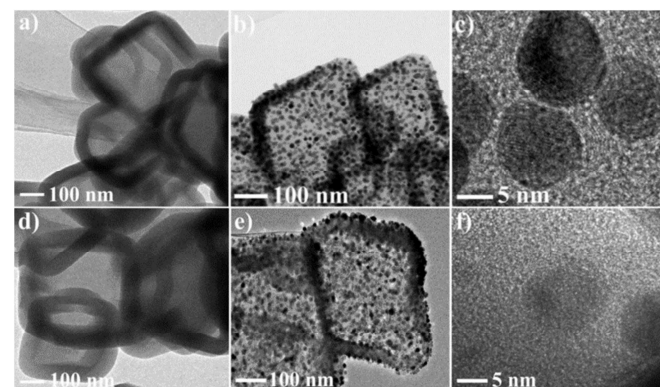
**Table 1.** The aerobic oxidation of hydrocarbons catalysed by Pd-Cu@HO-NPC.

Entry	Substrate	Product	Conv. <sup>b</sup> (%)	Select. <sup>b</sup> (%)
1			86	>99
2 <sup>c</sup>			< 1	-
3 <sup>d</sup>			-	-
4 <sup>e</sup>			50	>99
5 <sup>f</sup>			33	96
6 <sup>g</sup>			31	>99
7 <sup>g</sup>			31	>99
8			75	>97
9			71	>99
10			89	>99
11			38	>99
12			44	>93
13			29	>95
14			48	89
15 <sup>h</sup>			< 0.3	-

<sup>a</sup> Reaction conditions: hydrocarbons (1 mL), catalyst ([Pd] = 0.2 mol%), air flow (5 mL min<sup>-1</sup>), 120 °C and 24 h. <sup>b</sup> GC yield. <sup>c</sup> The absence of catalysts; <sup>d</sup> Pd-Cu@NPC was used as catalyst; <sup>e</sup> Under N<sub>2</sub> atmosphere; <sup>f</sup> Pd/C was used as catalyst; <sup>g</sup> Filtration experiment; <sup>h</sup> *p*-Benzoquinone was added (1 mmol).

This strategy for the synthesis of Pd-Cu@HO-NPC exhibits excellent generality, and can be extended to the fabrication of other Cu-based bimetallic and trimetallic alloy NPs. The treatment of HKUST-1@ImIP with aqueous K<sub>2</sub>PtCl<sub>6</sub> and Na<sub>2</sub>PdCl<sub>4</sub>/K<sub>2</sub>PtCl<sub>6</sub> solutions generated hollow Pt-Cu@HO-ImIP and Pd-Pd-Cu@HO-ImIP, respectively (Fig. 7a and 7d). Their morphology and size are almost identical with that of Pd-Cu@HO-ImIP, suggesting the change of exchanged metal ions has no obvious effects on the flexible ImIP shells. Notably, the pyrolysis of Pt-Cu@HO-ImIP and Pd-Pd-Cu@HO-ImIP under inert atmosphere gave rise to corresponding bimetallic Pt-Cu

and trimetallic Pd-Pt-Cu alloy NPs supported by hollow nitrogen-doped carbon shells. TEM analyses indicate that Pt-Cu@HO-NPC and Pd-Pt-Cu@HO-NPC also possess hollow octahedral morphology, the edge lengths and shell thickness are in the range of 200-500 nm and 30-60 nm, respectively (Fig. 7). The alloy NPs are tightly embedded in the HO-NPC shell, their size, location and distribution are very similar to those in Pd-Cu@HO-NPC.



**Fig. 7** TEM images for (a) Pt-Cu@HO-ImIP, (b, c) Pt-Cu@HO-NPC, (d) Pd-Pt-Cu@HO-ImIP and (e, f) Pd-Pt-Cu@HO-NPC.

## Conclusions

HKUST-1@ImIP core-shell materials have been fabricated and employed as promising precursors of Cu-based alloy NPs embedded in hollow nitrogen-doped porous carbon. HKUST-1 is simultaneously decomposed when metal-containing anions are introduced into the ImIP shell through anion exchange in water, no tedious steps and hazardous reagents are required for the removal of templates, the morphology and size of the flexible shell are well maintained. To the best of our knowledge, this is first report on hollow polymers with flexible backbones. The released Cu ions and exchanged metal ions reside in the pore of the ImIP shell, subsequent topotactic transformation generates hollow nitrogen-doped porous carbon incorporated with Cu-based bimetallic or trimetallic alloy NPs. The unique hollow structure endows metal alloy NPs with high catalytic activity and outstanding durability in selective aerobic oxidation of hydrocarbons. In summary, this study develops a simple, green and general method for facile synthesis of Cu-based alloy NPs supported by hollow carbon materials, the synthetic strategy holds great promises for the synthesis of a broad range of hollow carbon nanostructures owing to the availability of a large family of MOFs and ionic polymers, further investigation for other metal alloy NPs supported by various hollow heteroatom-doped carbon materials is on progress.

## Acknowledgements

This work was supported by the National Natural Science Foundation of China (21603228, 21673241 and 21471151), and the Strategic Priority Research Program of the Chinese Academy of Sciences (XDB20000000).





## Notes and references

- 1 G. H. Wang, J. Hilgert, F. H. Richter, F. Wang, H. J. Bongard, B. Spliethoff, C. Weidenthaler and F. Schüth, *Nat. Mater.*, 2014, **13**, 293-300.
- 2 X. H. Li and M. Antonietti, *Chem. Soc. Rev.*, 2013, **42**, 6593-6604.
- 3 L. Liu and A. Corma, *Chem. Rev.*, 2018, **118**, 4981-5079.
- 4 S. Li, A. Tuel, D. Laprune, F. Meunier and D. Farrusseng, *Chem. Mater.*, 2015, **27**, 276-282.
- 5 H. Yang, S. J. Bradley, A. Chan, G. I. N. Waterhouse, T. Nann, P. E. Kruger and S. G. Telfer, *J. Am. Chem. Soc.*, 2016, **138**, 11872-11881.
- 6 L. Chen, L. Zhang, Z. Chen, H. Liu, R. Luque and Y. Li, *Chem. Sci.*, 2016, **7**, 6015-6020.
- 7 B. Li, H. Nam, J. Zhao, J. Chang, N. Lingappan, F. Yao, T. H. Lee and Y. H. Lee, *Adv. Mater.*, 2017, **29**, 1605083.
- 8 W. Zhang, X. Jiang, Y. Zhao, A. Carne-Sanchez, V. Malgras, J. Kim, J. H. Kim, S. Wang, J. Liu, J. S. Jiang, Y. Yamauchi and M. Hu, *Chem. Sci.*, 2017, **8**, 3538-3546.
- 9 J. Liu, N. P. Wickramaratne, S. Z. Qiao and M. Jaroniec, *Nat. Mater.*, 2015, **14**, 763-774.
- 10 C. Chen, A. Wu, H. Yan, Y. Xiao, C. Tian and H. Fu, *Chem. Sci.*, 2018, **9**, 4746-4755.
- 11 W. Luo, M. Sankar, A. M. Beale, Q. He, C. J. Kiely, P. C. A. Bruijninx and B. M. Weckhuysen, *Nat. Commun.*, 2015, **6**, 6540.
- 12 H. Pan, Z. Cheng, Z. Xiao, X. Li and R. Wang, *Adv. Funct. Mater.*, 2017, **27**, 1703936.
- 13 J. Yang, F. Zhang, H. Lu, X. Hong, H. Jiang, Y. Wu and Y. Li, *Angew. Chem. Int. Ed.*, 2015, **54**, 10889-10893.
- 14 L. He, F. Weniger, H. Neumann and M. Beller, *Angew. Chem. Int. Ed.*, 2016, **55**, 12582-12594.
- 15 R. Jia, J. Chen, J. Zhao, J. Zheng, C. Song, L. Li and Z. Zhu, *J. Mater. Chem.*, 2010, **20**, 10829-10834.
- 16 Q. L. Zhu, J. Li and Q. Xu, *J. Am. Chem. Soc.*, 2013, **135**, 10210-10213.
- 17 L. T. Guo, Y. Y. Cai, J. M. Ge, Y. N. Zhang, L. H. Gong, X. H. Li, K. X. Wang, Q. Z. Ren, J. Su and J. S. Chen, *ACS Catal.*, 2015, **5**, 388-392.
- 18 J. Tang, J. Liu, R. R. Salunkhe, T. Wang and Y. Yamauchi, *Chem. Commun.*, 2016, **52**, 505-508.
- 19 Y. Wang, L. Yu and X. W. Lou, *Angew. Chem. Int. Ed.*, 2016, **55**, 14668-14672.
- 20 S. Yang, L. Peng, P. Huang, X. Wang, Y. Sun, C. Cao and W. Song, *Angew. Chem. Int. Ed.*, 2016, **55**, 4016-4020.
- 21 S. Yang, Y. Zhu, C. Cao, L. Peng, S. Li, D. Zhai and W. Song, *Nanoscale*, 2017, **9**, 13538-13545.
- 22 Y. Gong, H. Zhong, W. Liu, B. Zhang, S. Hu and R. Wang, *ACS Appl. Mater. Interfaces*, 2018, **10**, 776-786.
- 23 B. Xin and J. Hao, *Chem. Soc. Rev.*, 2014, **43**, 7171-7187.
- 24 B. Xin, C. Jia and X. Li, *Curr. Org. Chem.*, 2016, **20**, 616-628.
- 25 L. Zhang, H. B. Wu and X. W. Lou, *J. Am. Chem. Soc.*, 2013, **135**, 10664-10672.
- 26 J. Chun, S. Kang, N. Park, E. J. Park, X. Jin, K. D. Kim, H. O. Seo, S. M. Lee, H. J. Kim, W. H. Kwon, Y. K. Park, J. M. Kim, Y. D. Kim and S. U. Son, *J. Am. Chem. Soc.*, 2014, **136**, 6786-6789.
- 27 F. Zou, Y. M. Chen, K. Liu, Z. Yu, W. Liang, S. M. Bhaway, M. Gao and Y. Zhu, *ACS Nano*, 2016, **10**, 377-386.
- 28 J. Shao, Z. Wan, H. Liu, H. Zheng, T. Gao, M. Shen, Q. Qu and H. Zheng, *J. Mater. Chem. A*, 2014, **2**, 12194-12200.
- 29 X. Zhang, W. Qin, D. Li, D. Yan, B. Hu, Z. Sun and L. Pan, *Chem. Commun.*, 2015, **51**, 16413-16416. DOI: 10.1039/C5SC03531H
- 30 J. Yang, F. Zhang, H. Lu, X. Hong, H. Jiang, Y. Wu and Y. Li, *Angew. Chem. Int. Ed.*, 2015, **127**, 11039-11043.
- 31 P. Guo, D. Dutta, A. G. Wong-Foy and D. W. Gidley, *J. Am. Chem. Soc.*, 2015, **137**, 2651-2657.
- 32 Z. Hasan and S. H. Jhung, *J. Hazard. Mater.*, 2015, **283**, 329-339.
- 33 S. Zhang, H. Liu, P. Liu, Z. Yang, X. Feng, F. Huo and X. Lu, *Nanoscale*, 2015, **7**, 9411-9415.
- 34 C. Yu, J. Cui, Y. Wang, H. Zheng, J. Zhang, X. Shu, J. Liu, Y. Zhang and Y. Wu, *Appl. Surf. Sci.*, 2018, **439**, 11-17.
- 35 J. L. Zhuang, D. Ceglarek, S. Pethuraj and A. Terfort, *Adv. Funct. Mater.*, 2011, **21**, 1442-1447.
- 36 H. Zhao, X. Li, L. Li and R. Wang, *Small*, 2015, **11**, 3642-3647.
- 37 H. Zhong, C. Liu, Y. Wang, R. Wang and M. Hong, *Chem. Sci.*, 2016, **7**, 2188-2194.
- 38 J. S. Jang, W. T. Koo, S. J. Choi and I. D. Kim, *J. Am. Chem. Soc.*, 2017, **139**, 11868-11876.
- 39 J. Tang, R. R. Salunkhe, J. Liu, N. L. Torad, M. Imura, S. Furukawa and Y. Yamauchi, *J. Am. Chem. Soc.*, 2015, **137**, 1572-1580.
- 40 Z. P. Dong, X. D. Le, Y. S. Liu, C. X. Dong and J. Ma, *J. Mater. Chem. A*, 2014, **2**, 18775-18785.
- 41 K. Mori, H. Tanaka, M. Dojo, K. Yoshizawa and H. Yamashita, *Chem. Eur. J.*, 2015, **21**, 12085-12092.
- 42 M. Yuan, A. Liu, M. Zhao, W. Dong, T. Zhao, J. Wang and W. Tang, *Sens. Actuators, B Chem.*, 2014, **190**, 707-714.
- 43 F. Yang, Y. Zhang, P. F. Liu, Y. Cui, X. R. Ge and Q. S. Jing, *Int. J. Hydrogen Energy*, 2016, **41**, 6773-6780.
- 44 M. Hronec, K. Fulajtárová, I. Vávra, T. Soták, E. Dobrocka and M. Micusík, *Appl. Catal. B: Environ.*, 2016, **181**, 210-219.
- 45 X. Du, S. Luo, H. Du, M. Tang, X. Huang and P. K. Shen, *J. Mater. Chem. A*, 2016, **4**, 1579-1585.
- 46 L. Li, L. Li, C. Cui, H. Fan and R. Wang, *ChemSusChem*, 2017, **10**, 4921-4926.
- 47 X. Lin, Z. Nie, L. Zhang, S. Mei, Y. Chen, B. Zhang, R. Zhu and Z. Liu, *Green Chem.*, 2017, **19**, 2164-2173.
- 48 P. Zhang, Y. Gong, H. Li, Z. Chen and Y. Wang, *Nat. Commun.*, 2013, **4**, 1593.
- 49 T. Maegawa, A. Akashi, K. Yaguchi, Y. Iwasaki, M. Shigetsura, Y. Monguchi and H. Sajiki, *Chem. Eur. J.*, 2009, **15**, 6953-6963.
- 50 L. Kesavan, R. Tiruvalam, M. H. A. Rahim, M. I. B. Saiman, D. I. Enache, R. L. Jenkins, N. Dimitratos, J. A. Lopez-Sanchez, S. H. Taylor, D. W. Knight, C. J. Kiely and G. J. Hutchings, *Science*, 2011, **331**, 195-199.
- 51 D. Deng, Y. Yang, Y. Gong, Y. Li, X. Xu and Y. Wang, *Green Chem.*, 2013, **15**, 2525-2531.
- 52 M. Takahashi, H. Koizumi, W. J. Chun, M. Kori, T. Imaoka and K. Yamamoto, *Sci. Adv.*, 2017, **3**, e1700101.





## Table of Contents

HKUST-1 serves as a template of imidazolium-based ionic polymer, anion exchange and subsequent topotactic transformation generate hollow nitrogen-doped porous carbon incorporated with Cu-based alloy nanoparticles.

